Distinguishing between folding and tearing mechanisms in strange attractors

Greg Byrne[†], Robert Gilmore[†], and Christophe Letellier[‡]

[†] *Physics Department, Drexel University, Philadelphia, Pennsylvania 19104, USA*

[‡] *CORIA UMR 6614 - Université de Rouen, BP 12, Av. de l'Université, Saint-Etienne du Rouvray cedex, France*

(Dated: April 16, 2004, *Physical Review E*: To be submitted.)

We establish conditions for distinguishing between two topologically identical strange attractors that are enclosed by identical bounding tori, one of which is generated by a flow restricted to that torus, the other of which is generated by a flow in a different bounding torus and either imaged or lifted into the first bounding torus.

I. INTRODUCTION

The important properties of dynamical systems, and the strange attractors they may generate, are invariant under a smooth change of coordinates [1–3]. These include: the number and type of fixed points and their stability; geometric properties, such as fractal dimension; dynamical properties, such as Lyapunov exponents; and topological properties, such as topological entropy and the stretching and squeezing mechanisms that generate strange attractors. These mechanisms are understood in R^3, where they are described by branched manifolds. Branched manifolds summarize the stretching and squeezing mechanisms that act repetitively to build up strange attractors and to organize all their unstable periodic orbits in a unique way [4, 5]. For this reason they have been used to characterize low-dimensional strange attractors: those with Lyapunov dimension $d_L < 3$ [6].

Local diffeomorphisms identify n points ($n > 1$) in one phase space (R^3(cover)) with a single point in another phase space (R^3(image)) of the same dimension. Under a local diffeomorphism some of the properties of a strange attractor are preserved and others are not. The number of fixed points typically changes, while the stability of their images (or covers) does not; geometric properties, fractal properties, and topological entropy are preserved but global topological properties are not [7, 8].

Local diffeomorphisms are often related to symmetries. For example, if a dynamical system in R^3 is equivariant (unchanged) under rotations by π radians about the z-axis ($R_z(\pi)$) the $2 \to 1$ local diffeomorphism

$$\begin{aligned} u &= x^2 - y^2 \\ v &= 2xy \\ w &= z \end{aligned} \tag{1}$$

identifies pairs of rotation-related points off the z-axis in the covering phase space $R^3(x, y, z)$ with a single point in the image phase space $R^3(u, v, w)$ [7, 8]. This transformation maps a strange attractor with $R_z(\pi)$ symmetry to an image strange attractor without symmetry. The two attractors are locally identical. By the inverse process, an image attractor without symmetry (with variables (u, v, w)) can be "lifted" to a covering attractor with symmetry (and coordinates (x, y, z)).

In this work we investigate two related questions. (1) Suppose a covering attractor (Lorenz) is mapped to an image, so that it looks topologically like a Rössler attractor. How is it possible to distinguish this image from a Rössler attractor? (2) Suppose a Rössler attractor is lifted to a covering attractor. How is it possible to distinguish the lift from an attractor generated by an equivariant set of equations?

We resolve both questions by investigating the return maps of the attractors. These carry very clear signatures of the stretching and squeezing mechanisms that generate chaos. These are the stretching and folding mechanism that occurs in Rössler-like attractors, and stretching and tearing (and sometimes folding) mechanism, which occurs when a symmetry is present.

In Sec. II we study return maps for strange attractors generated by flows in a bounding torus of genus-1 [9, 10]. For highly dissipative dynamical systems these look like smooth curves with differentiable local extrema. In Sec. III we study return maps for strange attractors generated by flows with $R_z(\pi)$ symmetry. These flows exist in a torus of genus three. The Poincaré section consists of two generally disjoint components, and the return map describes how initial conditions on each component are mapped to these components [9, 10]. In Sec. IV we compare image dynamics with dynamics in a genus-one flow. The two differ in that for one the extrema in the return map are differentiable, for the other they are not. In Sec. V we compare covering dynamics with the dynamics of a typical strange attractor that can be generated in a genus-3 bounding torus. Return maps for both exhibit discontinuities. They differ in that in one case the one-sided derivatives at the discontinuity are equal, in the other case they are not. We summarize our results in Sec. VI.

II. RÖSSLER-LIKE DYNAMICS

We begin our study by constructing a return map for the Rössler attractor [11]. This is done in the usual way. The Rössler equations

$$\begin{aligned} \dot{x} &= -y - z \\ \dot{y} &= x + ay \\ \dot{z} &= b + z(x - c) \end{aligned} \tag{2}$$

are integrated for control parameter values $(a, b, c) = (0.432, 2.0, 4.0)$ to generate a strange attractor. Intersections y_i with the y-z plane through x_c (the x coordinate of the unstable focus near the origin) with $\dot{x} > 0$ are recorded and used to create a first return map y_{i+1} vs. y_i. This return map is shown in Fig. 1. The return map looks like a smooth, differentiable curve. In fact, it has such an appearance because the Rössler attractor is highly dissipative. More generally, such a return plot would exhibit some fuzziness since the attractor is fractal. If the strange attractor is first projected onto a branched manifold and the intersection of this branched manifold were used to create a first return map, the result would rigorously be a smooth, differentiable curve. Here and below we use the return map for an attractor in place of a return map for the branched manifold since there is almost no observable difference between the two in the cases that we study.

The return map shown in Fig. 1 has a quadratic maximum. This occurs because as the flow spirals outward from the unstable focus near the origin, it must decelerate before being reinjected towards the unstable focus. In fact, this is a common property of all strange attractors contained in a bounding torus of genus one that are generated by smooth flows [9, 10]. Each monotonic component of the return map can be identified with a branch of the characterizing branched manifold, and all monotonic segments are separated by a local maximum or minimum that is smooth, differentiable, and generically quadratic. Deceleration is responsible for horizontal tangents at extrema.

The mechanism responsible for creating chaos in the Rössler dynamical system and all similar dynamical systems (smooth forcing terms, strange attractor contained in a genus-1 torus) is stretching and folding. Differentiability of the return map at its critical points is the fingerprint characterizing folding.

III. LORENZ-LIKE DYNAMICS

The Lorenz equations [12]

$$\begin{aligned} \dot{x} &= -\sigma x + \sigma y \\ \dot{y} &= Rx - y - xz \\ \dot{z} &= -bz + xy \end{aligned} \tag{3}$$

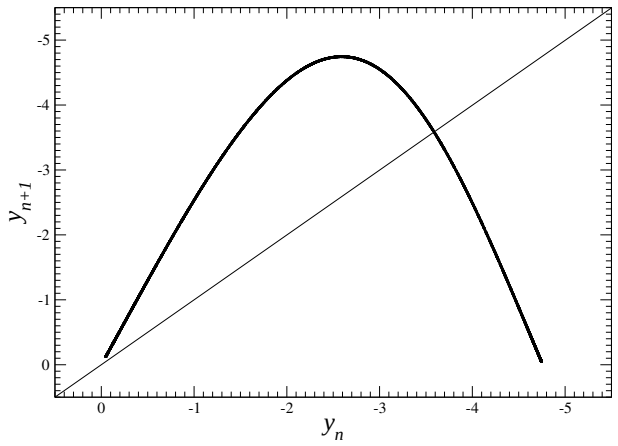

FIG. 1: First return map for the Rössler attractor. Parameter values: $(a, b, c) = (0.432, 2.0, 4.0)$.

were integrated for several different parameter values. Figs. 2(a) and 2(b) show projections of the Lorenz attractor generated with parameter values $(R, \sigma, b) = (28.0, 10.0, 8/3)$ onto the x-z and the x-y planes. This attractor can be contained in a bounding torus of genus three. The three (= genus) holes surround the two foci and the saddle at the origin. The global Poincaré section consists of two disconnected components. Both are shown in these figures. Fig. 2(c) shows a return mapping of the Poincaré section to itself. This return map shows that some of the initial conditions along the component of the Poincaré section near the focus on the left (L) return to the neighborhood of L (panel L-L), while initial conditions further away from this fixed point flow from L to R (panel L-R). Similar remarks hold, by symmetry, for flows originating on the component of the Poincaré section near the right hand focus R. The discontinuity in the flow from L (and R) is the fingerprint for the stretching and tearing mechanism. In this case, the flow from L accelerates away from L, and as it nears the origin, it is split into a part that returns to L and a part that flows to a different component of the Poincaré section. The origin serves as a splitting singularity. The branched manifold for this attractor has four branches, one each describing the flows from: $L \to L$, $L \to R$, $R \to L$, $R \to R$. Acceleration is responsible for non-horizontal tangents at extrema.

Fig. 3 is similar to Fig. 2, but for the Lorenz attractor generated for control parameter values $(R, \sigma, b) = (65.584, 13.0, 2.4167)$. The return map on the two components of the Poincaré section is shown in Fig. 3(c). In this case there is a discontinuity. It appears as the jump from L to R and the jump from R to L. Folding also occurs — it appears in the off-diagonal panels L-R and R-L in the return map. This return map shows clearly that the strange attractor, for these parameter values, is generated by both tearing and folding mechanisms.

Fig. 4 shows x-z and x-y projections of the Lorenz at-

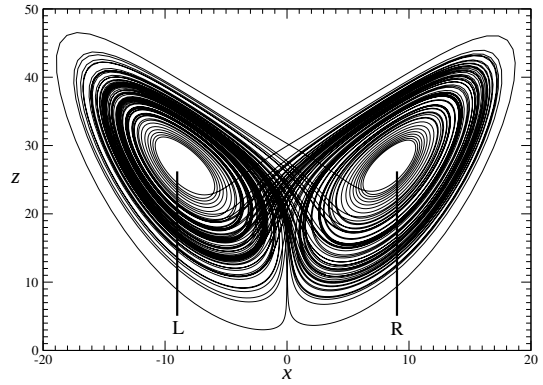

(a) x-z plane projection

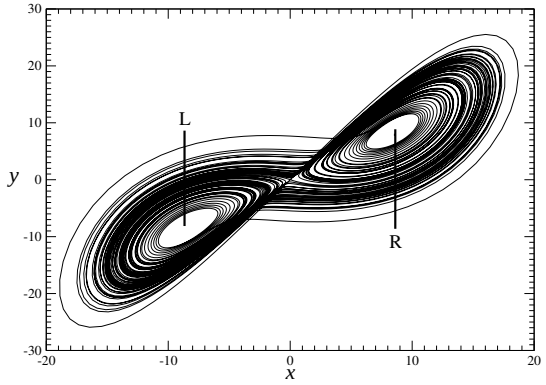

(b) x-y plane projection

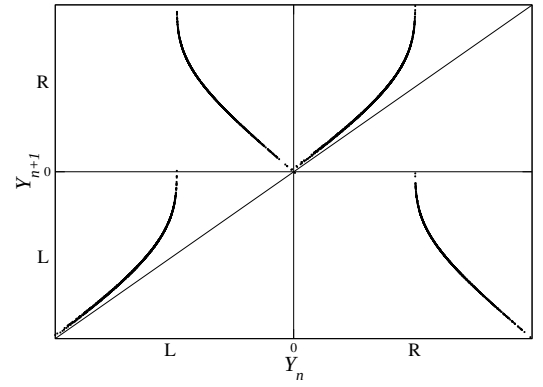

(c) First-return map

FIG. 2: Projection of the Lorenz attractor onto (a) the x-z plane and (b) the x-y plane. The two components of the global Poincaré section are shown. (c) Return map on the two components of the Poincaré section shows the branched manifold has four branchs. Tearing occurs. Parameter values: $(R, \sigma, b) = (28.0, 10.0, 8/3)$.

tractor generated for control parameter values $(R, \sigma, b) = (278.56, 30.0, 1.0)$. The first return map can be taken in two ways. If we use two disjoint commponents for a Poincaré section, as in the case shown in Fig. 2, the return map is as shown in Fig. 5(a). All initial conditions originating on L flow to R, and vice versa. This is a clear signature that one of the two components of the Poincaré section is superfluous. This is the case since the strange attractor can be enclosed in a bounding torus of genus-1. This can clearly be seen in Fig. 4(b). A single component (either L or R) suffices. The first return map on this single component is shown in Fig. 5(b). All extrema are differentiable, clearly indicating that this attractor is generated by folding, not tearing.

As we vary the control parameter values in the Lorenz attractor, we see that there is a transition in the mechanism that generates the strange attractor: from tearing alone (Fig. 2), to tearing and folding (Fig. 3), to folding alone (Fig. 4).

IV. IMAGE DYNAMICS

The transformation (1) can be used to map an attractor with rotation symmetry ($R_z(\pi)$) to an image attractor without symmetry. The Lorenz attractors shown in Figs. 2-4 were mapped to their $2 \to 1$ images using this $2 \to 1$ local diffeomorphism. The image attractors are shown in Figs. 6(a) - 8(a). Each attractor is enclosed in a genus-1 bounding torus, so that the global Poincaré surface of section consists of a single connected component. This component is shown explicitly in each of the Figs. 6(a)-8(a). The first return map of this Poincaré section onto itself is shown in Figs. 6(b) - 8(b). These three return maps differ in significant ways.

The return map shown in Fig. 6(b) shows two branches separated by a non-differentiable extremum. This is a clear signature that tearing occurs in the cover. The dynamical system in Fig. 6(a) is the image of a dynamical system in which tearing is responsible for generating chaotic behavior. The non differentiability of the return map at the local minimum is due to the cover singularity which has been mapped into the flow of the image.

The return map shown in Fig. 7(b) shows three branches. The three are separated by a non-differentiable maximum and a differentiable minimum. The maximum shows that tearing occurs in the cover, while the differentiable minimum shows that folding also occurs in the cover.

Finally, the return map shown in Fig. 8(b) shows two branches separated by a differentiable extremum. This attractor is generated by folding alone. It is not possible, in this case, to claim that this is the image of a covering attractor, since there is no evidence of tearing in this return map.

Bifurcation diagrams are simple to compute for simple systems and more complicated to compute for more

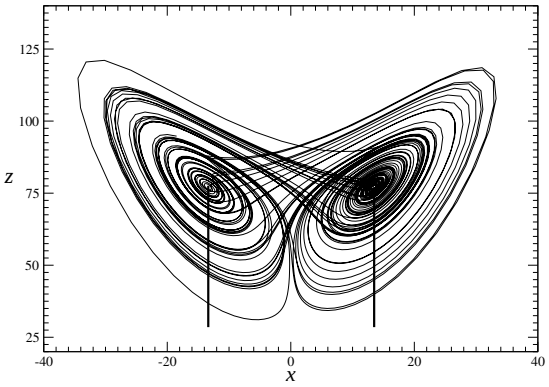

(a) x-z plane projection

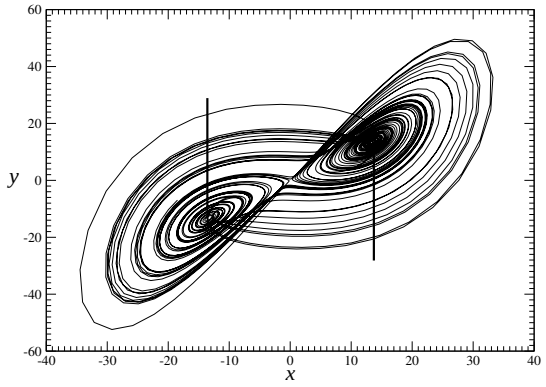

(b) x-y plane projection

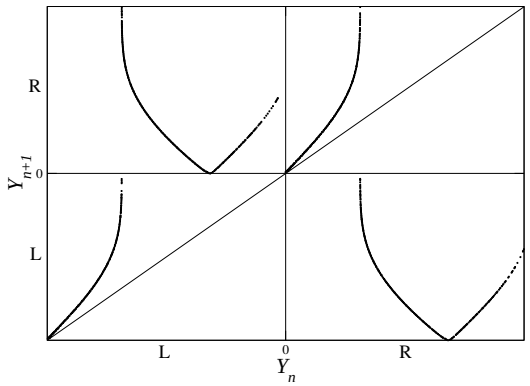

(c) First-return map

FIG. 3: Projection of the Lorenz attractor onto (a) the x-z plane and (b) the x-y plane. The two components of the global Poincaré section are shown. (c) Return map on the two components of the Poincaré section shows the branched manifold has six branchs. Tearing and folding occur. Parameter values: $(R, \sigma, b) = (65.584, 13.0, 2.4167)$.

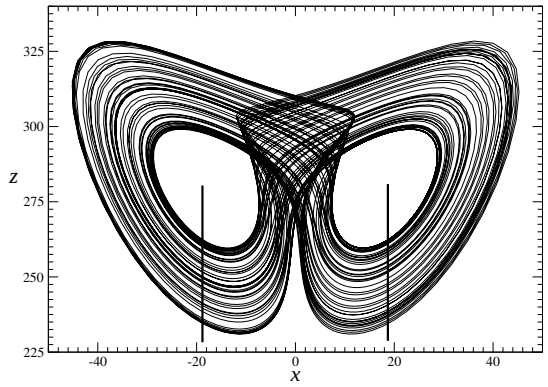

(a) x-z plane projection

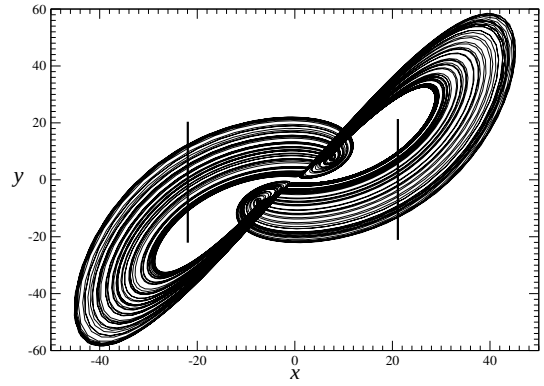

(b) x-y plane projection

FIG. 4: Projection of the Lorenz attractor onto (a) the x-z plane and (b) the x-y plane. Parameter values: $(R, \sigma, b) = (278.56, 30.0, 1.0)$.

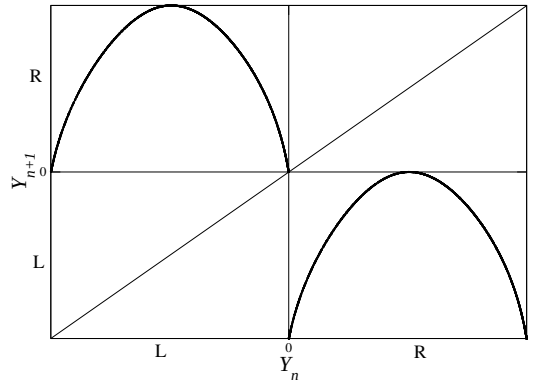

(a) Onto two components

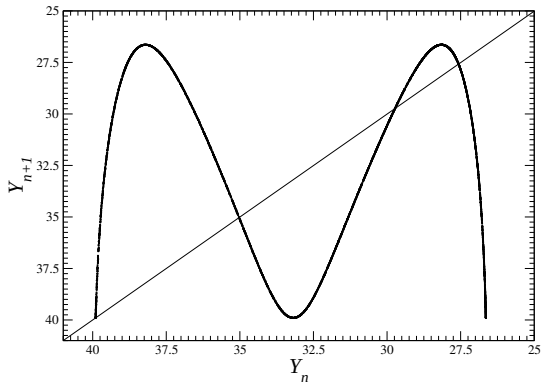

(b) Onto one component

FIG. 5: First return maps for the Lorenz attractor shown in Fig. 4. (a) The map onto the two components L and R shows that one component suffices. (b) The return map on a single component shows that stretching and folding is the operative mechanism. Both maps show the flow has four branches.

complex systems (genus > 1). We compute the bifurcation diagram for the Lorenz attractor as the control parameters are changed according to

$$\begin{aligned} R &= R_0 + \rho(R_1 - R_0) \\ \sigma &= \sigma_0 + \rho(\sigma_1 - \sigma_0) \\ b &= b_0 + \rho(b_1 - b_0) \end{aligned} \tag{4}$$

where ρ is varied between 0 and 1.3. The parameter triples are $(R, \sigma, b)_0 = (28.0, 10.0, 8/3)$ and $(R, \sigma, b)_1 = (278.56, 30.0, 1.0)$. The results are simply presented by displaying the bifurcation diagram for the $2 \to 1$ images of these equivariant systems. This is shown in Fig. 9. This diagram indicates three distinct regimes of behavior. Tearing occurs for $\rho < 1$ and folding occurs for $0.15 < \rho$. Both occur in the common range $0.15 < \rho < 1$. The image branched manifold exhibits 2, 3, and 2 branches in these three regions, respectively. The covers have twice as many branches.

The image of a symmetric attractor can sometimes be created without explicitly constructing a local diffeomorphism. This occurs when a strange attractor is constructed by embedding a nongeneric observable of the symmetric attractor. As a particular example, when the z variable of the Lorenz system is used to construct a strange attractor using any kind of embedding, the resulting strange attractor is enclosed in a genus-1 bounding torus and shows folding. However, its return map is similar to that shown in Fig. 6(a), clearly indicating that the fundamental mechanism generating chaos is tearing.

V. COVER DYNAMICS

Just as covering attractors can be projected to their images using (1) (or an analog for other symmetry), image attractors can be lifted to covers using the inverse mapping. For example, using (1) backwards, the Rössler attractor can be lifted to a double cover. In fact, it can be lifted to many topologically inequivalent double covers [8]. A sequence of three double covers of the Rössler attractor is shown in Figs. 10(a) - 12(a). These covers are all rotationally invariant under rotations $R_z(\pi)$ about the z axis. They differ from each other in the location of the rotation axis.

The cover shown in Fig. 10(a) is created from the Rössler attractor by inserting the rotation axis in the flow. Specifically, it is inserted in the "gap" between branches 0 and 1 in the Rössler attractor. With this nongeneric position of the z axis, the return map shown in Fig. 10(b) exhibits a jump at the point of horizontal tangency. The $R_z(\pi)$ equivariant double cover shown in Fig. 11(a) is constructed by inserting the z axis somewhere in the orientation preserving (0) branch of the Rössler attractor. In this case the jump from component L to R in the Poincaré section splits branch 0. The one-sided derivatives at the discontinuity are equal. This is the

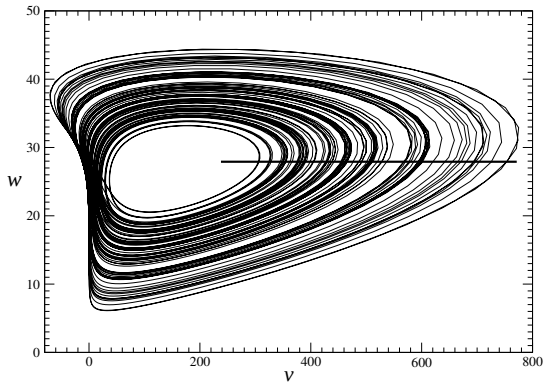

(a) v-w plane projection

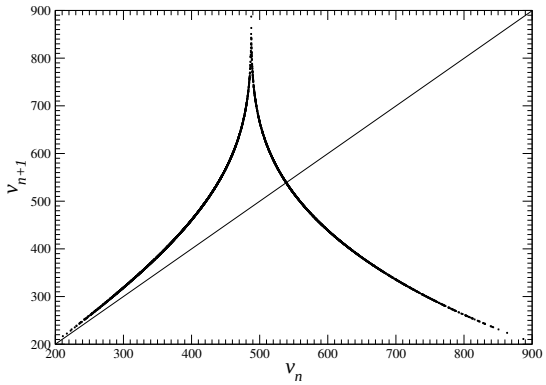

(b) First-return map

FIG. 6: (a) Projection of the $2 \mapsto 1$ image of the Lorenz attractor onto the v-w plane. The global Poincaré section has only the one component shown. First-return map on the Poincaré section shows the branched manifold has two branches. The return map is not differentiable everywhere, showing this is the image of a strange attractor where tearing occurs. Parameter values: $(R, \sigma, b) = (28.0, 10.0, 8/3)$.

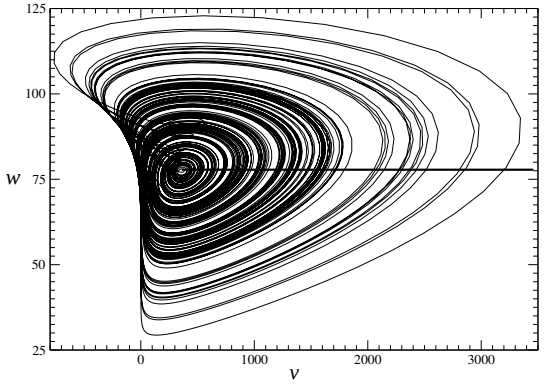

(a) v-w plane projection

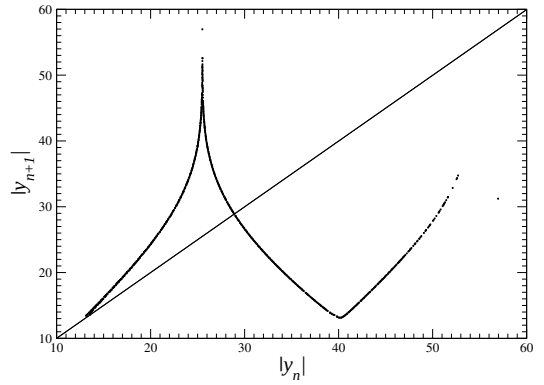

(b) First-return map

FIG. 7: (a) Projection of the $2 \mapsto 1$ image of the Lorenz attractor onto the v-w plane. The global Poincaré section has only the one component shown. First-return map on the Poincaré section shows the branched manifold has three branches. The return map is not differentiable everywhere, showing this is the image of a strange attractor where tearing occurs. The differentiable minimun shows that folding also occurs in the covering attractor. Parameter values: $(R, \sigma, b) = (65.584, 13, 2.4167)$.

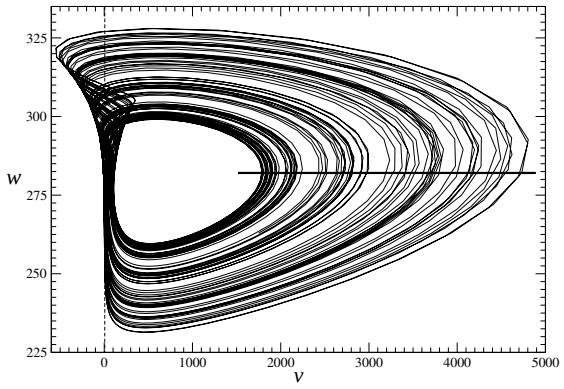

(a) v-w plane projection

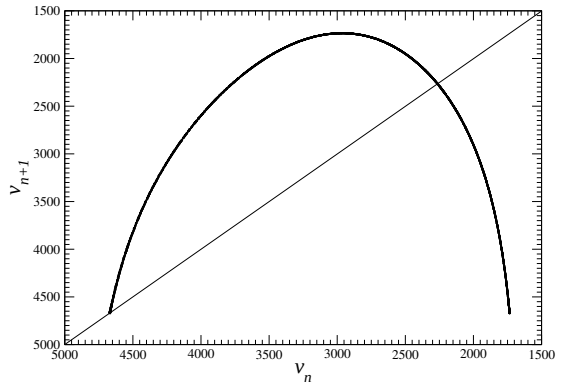

(b) First-return map

FIG. 8: (a) Projection of the $2 \mapsto 1$ image of the Lorenz attractor onto the v-w plane. The global Poincaré section has only the one component shown. First-return map on the Poincaré section shows the branched manifold has two branches. The return map is differentiable everywhere, showing this is a strange attractor where folding occurs. Parameter values: $(R, \sigma, b) = (278.56, 30.0, 1.0)$.

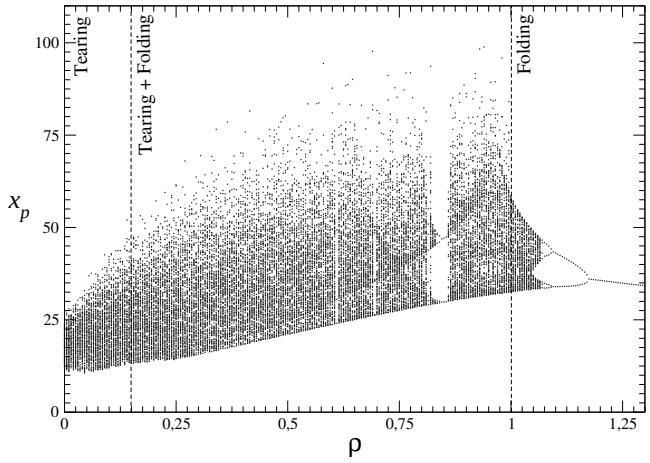

FIG. 9: Bifurcation diagram for the image of the Lorenz attractor, with $|x|$ plotted as a function of ρ.

signature that the cover is the lift of a strange attractor. The two one-sided derivatives at the jump shown in the return map of Fig. 10(b) are also equal, both equal to zero in that case. The two covers, shown in Figs. 10(a) and 11(a), are both enclosed by genus-3 bounding tori.

The double cover shown in Fig. 12(a) is created by inserting the symmetry axis inside the "hole" in the Rössler attractor. This cover has topological index $(n_0, n_1) = (1, 1)$ [8]. It can be enclosed in a genus-1 bounding torus. The global Poincaré section has a single connected component. This is shown in Fig. 12(a). The return map on this component is shown in Fig. 12(b). This shows four branches separated by three quadratic extrema. This strange attractor is created by the stretching and squeezing mechanism. From this return map, it is not possible to infer that this strange attractor is the lift of an image attractor, as no discontinuities are present.

VI. SUMMARY

We have described the fingerprints that can be used to identify the origin of low dimensisonal strange attractors when they are mapped among themselves by local diffeomorphisms. These fingerprints were explained in terms of examples using the Rössler and the Lorenz attractors and simple symmetry groups, but the results are independent of the particular dynamical system and the symmetry group used to create the local diffeomorphism. It is assumed that the source terms for the dynamical systems are smooth.

We can distinguish between the image of an attractor enclosed in a genus-g bounding torus ($g \geq 3$) and an attractor generated by smooth forcing terms in a genus-one attractor by the degree of smoothness of the first return map. If the map is not differentiable at some extremum, it is an image.

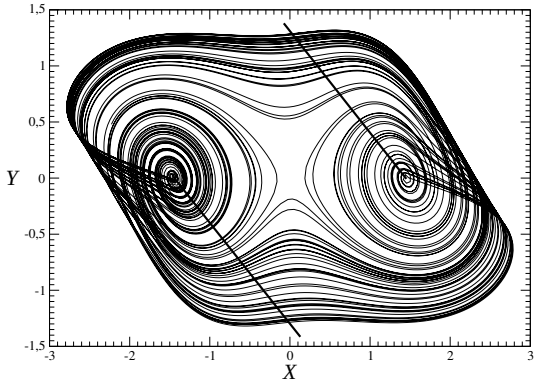

(a) X-Y plane projection

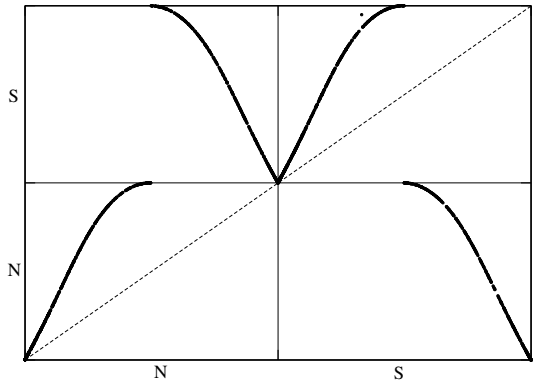

(b) First-return map

FIG. 10: (a) This double cover of the Rössler attractor can be enclosed in a genus-three bounding torus. The Poincaré section has a two components. (b) First-return map on the Poincaré section has four panels. The discontinuity in the return map shows that this strange attractor is generated by stretching and tearing. The equality of the slopes at the discontinuity shows that it is the lift of a strange attractor generated in a bounding torus of genus one. This strange attractor is described by a branched manifold with four branches. Parameter values: $(a, b, c) = (0.432, 2.0, 4.0)$.

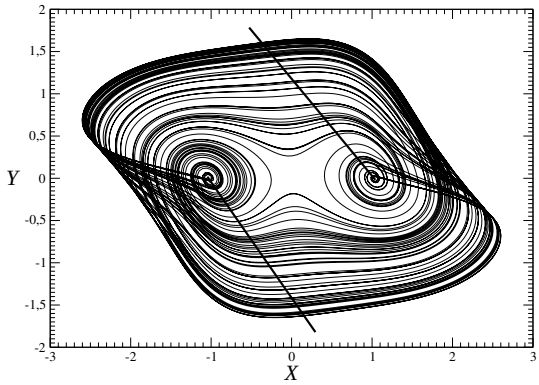

(a) X-Y plane projection

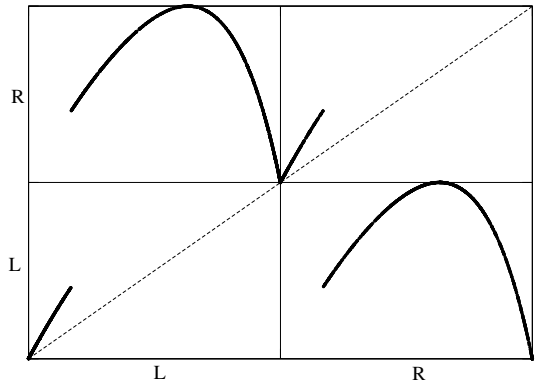

(b) First-return map

FIG. 11: (a) Another double cover of the Rössler attractor. This can also be enclosed in a genus-three bounding torus. (b) The discontinuity in the return map shows that this strange attractor is generated by stretching and tearing. The differentiable maxima show that folding also takes place. The equality of the slopes at the discontinuity shows that it is the lift of a strange attractor generated in a bounding torus of genus one. This strange attractor is described by a branched manifold with six branches. Parameter values: $(a, b, c) = (0.432, 2.0, 4.0)$.

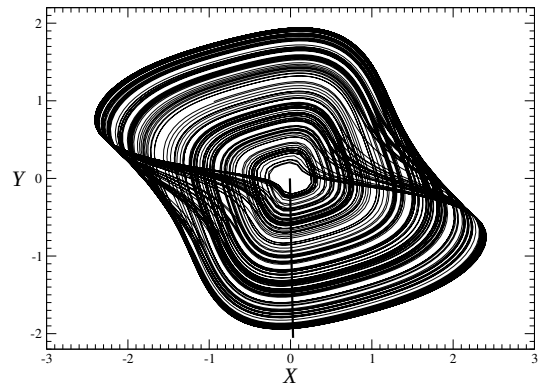

(a) X-Y plane projection

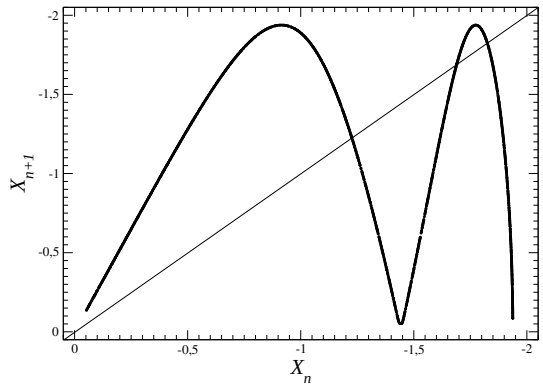

(b) First-return map

FIG. 12: (a) One double cover of the Rössler attractor that can be enclosed in a genus-one bounding torus. The Poincaré section has a single component. (b) First-return map on the Poincaré section. This strange attractor is generated by stretching and folding, and is described by a branched manifold with four branches. Parameter values: $(a, b, c) = (0.432, 2.0, 4.0)$.

Covers that can be enclosed in a genus-g bounding torus are described by their return maps on a global Poincaré section. The section has exactly $g - 1$ components, usually disjoint [9, 10]. Discontinuities show where tearing takes place. Tearing is due to the presence of saddle splitting points. Differentiable maxima show that folding also takes place. Equality of the two one-sided derivatives at a discontinuity shows that the cover is the lift of a strange attractor whose return map is differentiable — that is, a strange attractor generated by smooth forcing functions in a genus-one bounding torus.

We thank T. D. Tsankov and A. Nishtala for useful comments. This work was supported in part by NSF Grant PHY9987468.

REFERENCES

[1] H. G. Solari, M. A. Natiello, and G. B. Mindlin, *Nonlinear Dynamics: A Two-Way Trip from Physics to Math*, (IOP Publishers, London, 1996).
[2] N. B. Tufillaro, T. Abbott, and J. Reilly, *An Experimental Approach to Nonlinear Dynamics and Chaos*, (Addison-Wesley, Reading, MA, 1992).
[3] E. Ott, *Chaos in Dynamical Systems*, (Cambridge University Press, Cambridge, 1993).
[4] J. Birman and R. F. Williams, Topology **22**, 47-82 (1983).
[5] J. Birman and R. F. Williams, Cont. Math. **20**, 1-60 (1983).
[6] R. Gilmore and M. Lefranc, *The Topology of Chaos*, NY: Wiley, 2002.
[7] R. Miranda and E. Stone, Phys. Lett. A**178**, 105 (1993).
[8] C. Letellier & R. Gilmore, Physical Review E, **63**, 16206, (2001).
[9] T. D. Tsankov and R. Gilmore, Phys. Rev. Lett. **91**(13), 134104 (2003).
[10] T. D. Tsankov and R. Gilmore (unpublished).
[11] O. E. Rössler, Phys. Lett. A**57**, 397 (1976).
[12] E. N. Lorenz, J. Atmos. Sci. **20**, 130 (1963).